Intragap states in SmB_6

N. E. Sluchanko, V. V. Glushkov, B. P. Gorshunov,* S. V. Demishev, M. V. Kondrin, A. A. Pronin, and A. A. Volkov
General Physics Institute, Russian Academy of Sciences, Vavilov Strasse 38, 117942, Moscow, Russia

A. K. Savchenko
Physics Department, University of Exeter, Stocker Road, Exeter EX4 4QL, United Kingdom

G. Grüner
Department of Physics and Solid State Science Center, University of California at Los Angeles, Los Angeles, California 90024

Y. Bruynseraede and V. V. Moshchalkov
Laboratory voor Vaste-Stoffysica en Magnetisme, K. U. Leuven, Celestijnenlaan 200, B-3001 Leuven, Belgium

S. Kunii
Department of Physics, Tohoku University, Sendai 980, Japan
(Received 14 September 1999)

The results of wide-range measurements of the low-frequency, rf, and microwave conductivity in the typical mixed-valent narrow-gap semiconductor samarium hexaboride are presented. The established steplike anomaly of conductivity $\sigma(\nu)$ around 10 GHz is discussed in the framework of the exciton-polaron approach and coherent-state formation in SmB_6 at helium temperatures. A combined analysis of the dc- and wide-range ac-transport characteristics and dielectric permittivity data at low temperatures is developed.

Samarium hexaboride is a prototypical member of a class of intermediate-valence compounds, the narrow-gap semiconductors. Gap formation in these materials is thought to originate from the hybridization of the narrow f band with broad enough s,p,d-type conduction bands, with each unit cell containing an even number of electrons. Although SmB_6 has been studied comprehensively for about three decades, since the 1970s,[1] all the questions about the origin of the intragap states and the mechanisms of low-temperature conductivity in this very interesting and intriguing material are still not fully answered.[2–3]

Moreover, only very recently have direct measurements been performed of the low-temperature dynamical conductivity $\sigma(\nu)$ and dielectric permittivity $\epsilon(\nu)$ in SmB_6 single crystals in the spectral range from 0.6 to 4.5 meV,[4] i.e., below the hybridization gap. The results obtained[4] together with the data from low-temperature transport measurements[5] give evidence of an indirect energy gap of about 20 meV in the density of states. Additionally, ''impurity states'' have been found at $E_{ex} \approx 3.5$ meV below the bottom of the conduction band.[4] However, only a few microscopic parameters of the charge carriers have been determined so far.[4,5]

An essential difference between dc and submillimeter-range conductivity (by a factor of 100) has been established for samarium hexaboride at low temperatures $T \leqslant T_m \approx 5$ K (Ref. 4; see also curves 1 and 3 in Fig. 1). The appearance of the discrepancy between σ_{sbmm} and σ_{dc} is accompanied by a transition to a ''metalliclike behavior'' of the Seebeck and Hall coefficients (Fig. 1, curves 4 and 5; see also Ref. 5). Moreover, a number of significant changes in thermodynamic and kinetic characteristics such as the thermal expansion coefficient,[6] NMR spin-lattice relaxation rate,[7] magnetoresistance,[8] and elastic modulus C_{11},[9] etc., can evidently be understood in terms of an electronic phase transition at $T_m \approx 5$ K.[5]

From this point of view the investigation of the frequency-dependent difference $\sigma_{sbmm} - \sigma_{dc}$ at low temperatures should probably be the key experiment to shed light on the origin of the extraordinary ground state of SmB_6. Therefore, comprehensive measurements of the low-frequency, rf, and microwave conductivity in samarium hexaboride have been carried out in the present study, and the results obtained allow us to develop a combined analysis of the dc- and wide-range ac-transport characteristics and dielectric permittivity $\epsilon(T)$ at low temperatures.

Single-crystal samples from the same ingot as in Refs. 4 and 5 were used in the investigation. Special attention was focused on the preparation of the sample surface[10] and the contacts for performing the resistance and impedance measurements. The dc Hall voltage and the ac (3 Hz–50 kHz) resistivity were measured by the Van der Pauw four-probe method with a low-frequency lock-in amplifier technique. Using a HP 4191A rf impedance analyzer, radio frequency experiments in the range 1 MHz–1 GHz were performed with a short enough semirigid coaxial line with the help of a cryostat assembly of original design. The electrodynamical response of SmB_6 in the millimeter wave range of frequency (35 GHz) has been studied by the microwave cavity perturbation technique.[11]

The ac-conductivity measurements have been carried out within a very wide (of about nine orders of magnitude) frequency range at temperatures below the electronic phase transition $T \leqslant T_m \approx 5$ K. The data obtained are presented in Fig. 2 (upper panel) together with submillimeter and optical conductivity results (Refs. 3 and 4). The established dramatic

 ©2000 The American Physical Society

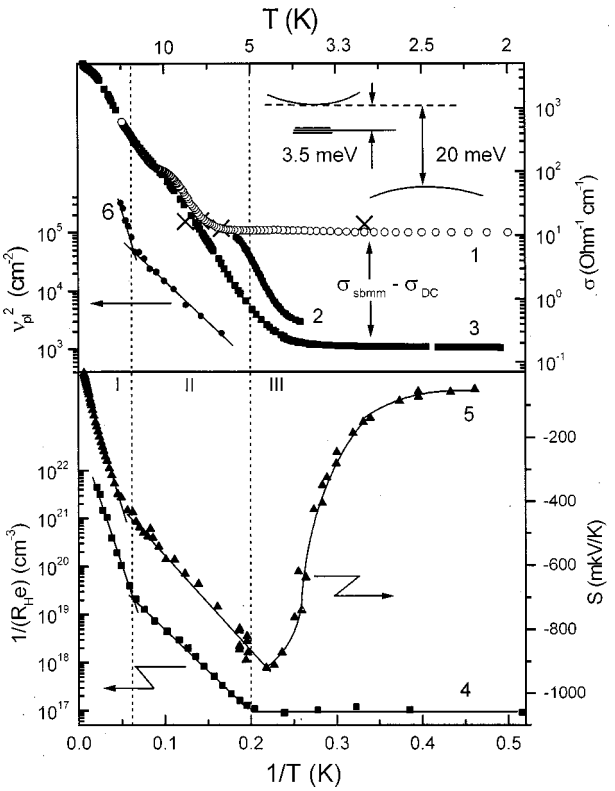

FIG. 1. Temperature dependence of conductivity $\sigma(T,\nu_0)$ at fixed frequencies. (1) ○, $\nu_0=35$ GHz, X, 480 GHz; (2) 900 MHz; (3) dc results. Additionally the temperature dependence of the reciprocal Hall $[eR_H(T)]^{-1}$ (curve 4) and Seebeck $S(T)$ (curve 5) coefficients from Ref. 5 and the squared plasma frequency $\nu_{\rm pl}^2(T)$ (curve 6) from Ref. 4 of SmB_6 are shown. The temperature intervals I, II, and III correspond to intrinsic conduction ($T\geqslant 14$ K), the ''impurity scattering'' region (5–14 K), and the coherent state ($T\leqslant T_m\approx 5$ K), respectively. The inset gives a simplified view of the band structure of SmB_6.

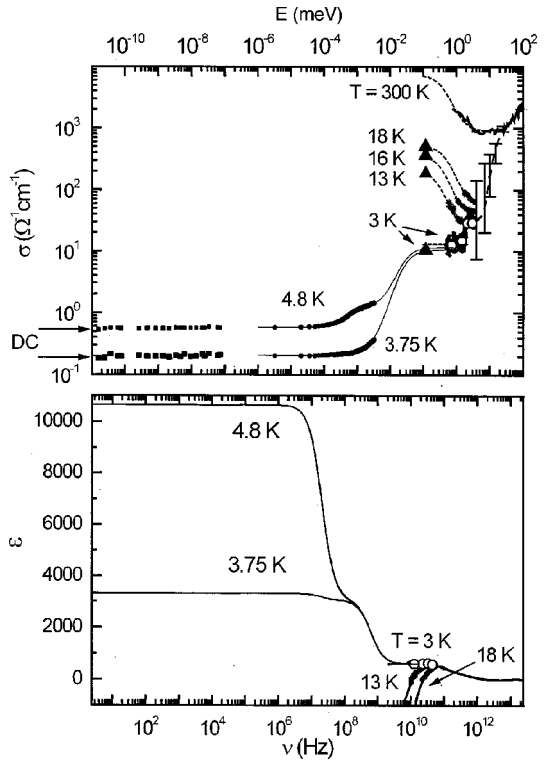

FIG. 2. Frequency-dependent conductivity $\sigma(\nu)$ (upper panel) and dielectric permittivity $\epsilon(\nu)$ (lower panel) of SmB_6 at different temperatures. The solid lines in the upper panel show a fit with one ($T=3.75$ K) and two ($T=4.8$ K) Debye relaxator terms, which allowed us to estimate the dielectric contributions (shown by solid lines in the lower panel) produced by the conductivity step at around 10 GHz.

decrease of low-temperature conductivity happens in the frequency interval 0.5–20 GHz, where the conductivity changes between $\sigma_{\rm sbmm}\approx 13\,\Omega^{-1}\,{\rm cm}^{-1}$ and $\sigma_{\rm dc}\approx 0.1\,\Omega^{-1}\,{\rm cm}^{-1}$ (Figs. 1 and 2). An essential change in the $\sigma_{\rm ac}(T,\nu_0)$ dependencies at fixed frequency ν_0 can be detected in the interval 100–1000 MHz (see Fig. 1, curves 1 and 2) although the conductivity activation energy is approximately the same as for the low-frequency range. At low frequencies $\nu\leqslant 50$ MHz, the ac-conductivity variation $\sigma(\nu)$ is negligible in abrogating any hopping transport interpretation in the low-temperature interval $T<5$ K for SmB_6. Moreover, the appearance of the $\sigma(\nu)$ steplike anomaly (Fig. 2) for $T<5$ K in combination with the ''metalliclike behavior'' of transport and thermodynamical parameters[1–10] certainly can be considered as the imprint of coherent-state formation in samarium hexaboride at liquid helium temperatures $T\leqslant T_m\approx 5$ K. On the other hand, the existence of the narrow f-d bands in the near vicinity of the Fermi energy E_F probably allows one to discuss the $\sigma(\nu)$ anomaly in terms of a manifestation of heavy-fermion transport and the appearance of a correlation gap in the high enough f-d-type density of states of the intermediate-valence compound. To distinguish between different mechanisms that can be used to describe this class of phenomenon, it is necessary to analyze consistently the low-temperature transport parameters of samarium hexaboride.

In the intrinsic conduction region $T\geqslant 14$ K (Ref. 5; see region I in Fig. 1) the experimental results for conductivity $\sigma(T)$ and the Seebeck $S(T)$ and Hall $R_H(T)$ coefficients (Fig. 1, curves 3–5) can be described in the framework of a phenomenological semiconductor approach:

$$S=\frac{k_B}{e}\left(\frac{b-1}{b+1}\,\frac{E_g}{2k_BT}+\frac{3}{4}\ln\frac{m_n}{m_p}\right), \tag{1}$$

$$\mu_n-\mu_p=R_H\sigma, \tag{2}$$

$$\ln|R_H|\sim E_g/2k_BT, \tag{3}$$

where E_g is the gap energy, $b=\mu_n/\mu_p,\mu_n,m_n,\mu_p,m_p$ are the electron and hole mobility and effective masses, respectively, k_B is the Boltzmann constant, and e is the charge of the electron. From a comparison between the slopes of $S\sim 1/T$ and $\ln|R_H|\sim 1/T$ (Fig. 1, curves 4 and 5) the ratio $b=\mu_n/\mu_p\approx 50$ can be deduced, and then the $\mu_n(T)$ and $\mu_p(T)$ dependencies can be directly evaluated from Eq. (2) and the experimental results of Fig. 1, curves 3 and 4. Moreover, in application of the plasma frequency behavior $\nu_{\rm pl}^2(T)$ of conductive electrons from Ref. 4 (see curve 6 in Fig. 1) one can expect to estimate the effective mass $m_n^*(T)$ and relaxation time $\langle\tau_n\rangle$ of the electrons, which are given by the simple expressions

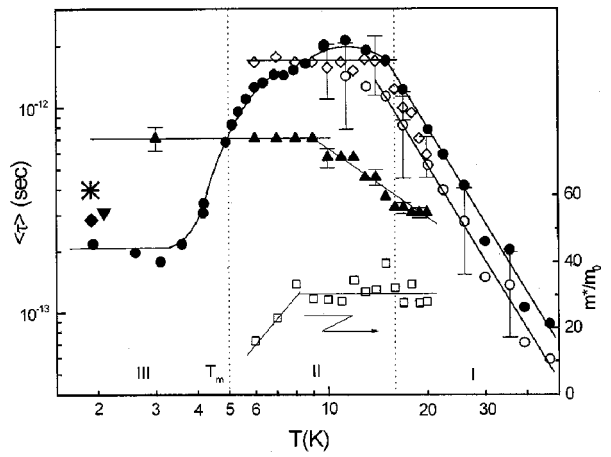

FIG. 3. Temperature dependence of effective mass $m_n^*(T)$ (□) and the relaxation time $\langle \tau_{n,p} \rangle$ as deduced from dc-transport measurements (● electrons and ○ holes) and as calculated from the analysis of the contributions from the Drude conductivity σ_{Drude} (◇) and the conductivity peak at 24 cm^{-1} σ_{osc} (▲) together with the relaxation rate parameters of NMR (Ref. 7) (◆), inelastic neutron scattering experiments (Ref. 14) (▼), and ultrasonic attenuation measurements (Ref. 9) (*). The temperature intervals I, II, and III correspond to intrinsic conduction ($T \geqslant 14$ K), the ''impurity scattering'' region (5–14 K), and the coherent state ($T \leqslant T_m \approx 5$ K), respectively.

$$\nu_{\text{pl}}^2(T) = Ne^2/\pi m_n^*(T), \tag{4}$$

$$\mu_{n,p} = e\langle \tau_{n,p} \rangle / m_{n,p}^* \tag{5}$$

Both of the $m_n^*(T)$ and $\langle \tau_n \rangle(T)$ parameters estimated from the experimental results of Fig. 1 in this manner are presented in Fig. 3. Additionally, the reciprocal damping rate calculated from the Drude term of the conductivity in the submillimeter range[4] is shown in Fig. 3, together with the reciprocal oscillator damping rate of the peak anomaly in $\sigma(\nu)$ that was observed in SmB_6 at the energies $E_{\text{peak}} \approx 3$ meV.[4] To complete the set of characteristics of the charge carriers, it is possible to estimate the $\langle \tau_p \rangle(T)$ parameter by using the value for the heavy charge carriers' ($4f$ holes) effective mass $m_p^* = (1000 \pm 500) m_0$, which was obtained in Ref. 12 from optical plasma resonance measurements. The $\langle \tau_p \rangle(T)$ dependence is shown in Fig. 3 and as could be expected from the nature of the charge fluctuation phenomena, these two parameters $\langle \tau_n \rangle(T)$ and $\langle \tau_p \rangle(T)$ are practically the same, at least within the limits of experimental accuracy.

One of the most important parameters that can be estimated from our data (Figs. 1–3) is the localization radius of ''the impurity states'':

$$a^* = \hbar / \sqrt{2 m_n^* E_{\text{ex}}}. \tag{6}$$

Using the values $E_{\text{ex}} \approx 3.5$ meV and $m_n^* \approx 30 m_0$ (Fig. 3) we calculated the small $a^* \approx 6$ Å value for these intragap states in SmB_6. The small value of the localization radius serves as an argument in favor of interpreting the low-temperature properties of SmB_6 within the Kikoin-Mishchenko exciton-polaron model.[13] In developing the approach of these authors[13] for application to analysis of the experimental results Figs. 1–3 we assume that the states at $E_{\text{ex}} \approx 3.5$ meV correspond to the formation of short-range excitons in the vicinity of Sm centers as a consequence of fast valence fluctuations of $4f$ electrons in SmB_6 at intermediate temperatures $T > 5$ K. It is interesting to compare the proposed interpretation with the result of inelastic neutron scattering experiments,[14] where the maximum of electron density has been estimated at a distance of about 1.5–2 Å from the Sm sites in the direction of the neighboring boron octahedra. Moreover, from the low-temperature ($T \approx 2$ K) data the authors[14] suggested the presence of interaction between these short-range ''excitonic clouds'' formed around each Sm ion in SmB_6. In addition, to add an argument against the correlation-gap Δ interpretation of the low-temperature ($T < 5$ K) anomalies in SmB_6, it is necessary to point out also the very small Δ value ($\Delta \sim h\nu \sim 0.01$ meV) that can be established from the $\sigma(\nu)$ steplike anomaly at liquid helium temperatures (Fig. 2, upper panel).

On the other hand, the application of the exciton-polaron concept in SmB_6 allows one to consider the low-temperature ''metallization'' at about $T_m \approx 5$ K as a transition to a coherent state with strongly interacting exciton-polaron complexes. There are a few models of interacting excitons that could be appropriate to describe the experimental results (Figs. 1–3) within the exciton condensation phase at $T \leqslant T_m \approx 5$ K. Among them the mechanism of electron-hole droplet formation at liquid helium temperatures in SmB_6 has been discussed qualitatively in Ref. 5. Unlike the photogenerated electron-hole liquid in classical semiconductors,[15] in the case of SmB_6 the fast charge fluctuations at each Sm center may serve as a source of short-range excitons in a large concentration ($\sim 10^{22}\,\text{cm}^{-3}$). Indeed, the calculated value of the critical concentration for condensed phase formation $n_c \sim a^{*-3} \approx 5 \times 10^{21}\,\text{cm}^{-3}$ does not allow us to exclude the electron-hole droplet interpretation. In our previous paper,[5] the wrong value of effective mass $m_n^* \approx 100 m_0$ was used to estimate the excitonic state parameters.

Another approach has been executed recently in the framework of the Falikov-Kimbal model to describe the ground-state formation of intermediate-valence compounds.[16] Bose-Einstein condensation of excitons was predicted in Ref. 16 for SmB_6 accompanied by a second-order ferroelectric phase transition and the appearance of ferroelectric resonance together with a threshold singularity in the infrared absorption spectrum. These authors[16] predict a dramatic enhancement of the polarization due to electronic-type ferroelectricity in SmB_6. Divergence of the static dielectric constant in the direction of spontaneous polarization and a critical behavior for a temperature-driven transition[16] could be verified by a Kramers-Kronig analysis of the wide-range $\sigma(\nu)$ results (Fig. 2, upper panel) in combination with direct radio frequency capacitance $C(T)$ measurements. Avoiding the known problems of Kramers-Kronig analysis (limitation and uncertainties due to extrapolations) the Debye relaxator terms have been used to estimate the dielectric contributions produced by the conductivity steps at around 10 GHz (Fig. 2, lower panel). The results of the $\sigma(\nu)$ fit with one ($T = 3.75$ K) and two ($T = 4.8$ K) Debye relaxator terms presented in Fig. 2 are in good agreement with the concept of electronic ferroelectricity.[16] It is worth emphasizing the ex-

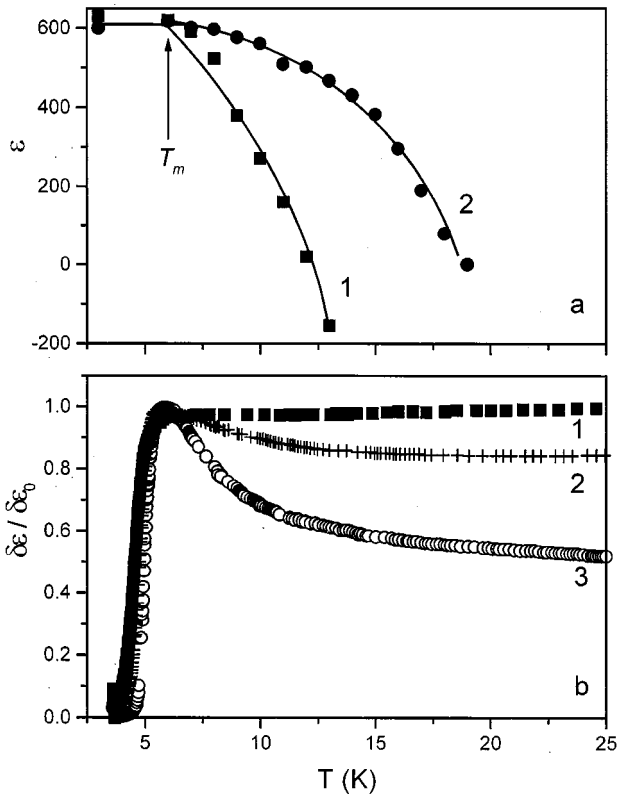

FIG. 4. The dielectric constant temperature dependence as detected (see text) from (a) quasioptical investigations (Ref. 4): (1) $\nu = 162$ GHz; (2) 480 GHz. (b) rf capacitance $C(T)$ measurements: (1) 130 MHz; (2) 450 MHz; (3) 900 MHz.

traordinary high values of dielectric constant ϵ in the near vicinity of the phase transition temperature: $\epsilon \approx 10\,000 - 15\,000$ (Fig. 2, lower panel) depending on the sample quality. In addition, the predicted λ-type anomaly of the dielectric permittivity is very sensitive to the radiation frequency (see also Fig. 2, lower panel) and does not occur for high-frequency $\epsilon(T)$ results [millimeter and submillimeter range, see Fig. 4(a)].

Direct radio frequency capacitance $C(T)$ measurements of SmB_6 have been carried out with a HP 4191 A rf impedance analyzer with low-temperature assembly. To avoid the equipment limitations that occur for radio frequency capacitance measurements of the highly conductive SmB_6 samples, a schema with two additional calibrated capacitors in series with the sample has been applied to estimate roughly the $\Delta C/C \sim \Delta\epsilon/\epsilon$ behavior. Despite the strong influence of the schema parameters on the experimental results, the electronic phase transition can certainly be detected at $T \approx 5$ K [see Fig. 4(b)]. Moreover, the data obtained [Fig. 4(b)] can be considered rather in support of a noticeable increase of the dielectric permittivity $\epsilon(T)$ in the vicinity of the electronic transition temperature $T \approx 5$ K in SmB_6.

In summary, the results of wide-range ac-conductivity measurements are reported for SmB_6 single crystals at helium temperatures. A comprehensive analysis of the low-temperature dc- and ac-transport characteristics in combination with recent quasioptical data[4] and the well-known thermodynamic properties of SmB_6 suggests interpretation of the data in the framework of the Kikoin-Mishchenko exciton-polaron model. In developing the approach a discussion in terms of the different scenarios for coherent ground state formation is presented.

The authors are grateful to Professor M. Dressel and Professor A. Loidl for numerous helpful discussions. This work was supported by the INTAS Program No. 96-451, Grant No. 17163 of the Russian Foundation for Basic Research, Programs ''Fundamental Spectroscopy'' and ''Microwaves'' of the Russian Ministry of Science and Technology, Research Grant No. 96929 of the President of Russian Federation, and Copernicus Network No. ERB IC15 CT98 0812.

*Present address: 1 Physikalisches Institut, Universitaet Stuttgart, D-70550 Stuttgart, Germany.

[1] V. C. Nickerson *et al.*, Phys. Rev. B **3**, 2030 (1971).
[2] G. Aeppli and Z. Fisk, Comments Condens. Matter Phys. **16**, 155 (1992).
[3] P. Wachter, in *Handbook on the Physics and Chemistry of Rare Earths*, edited by K. A. Gschneidner, Jr., L. Eyring, G. H. Lander, and G. R. Choppin (Elsevier, Amsterdam, 1994), Vol. 19.
[4] B. Gorshunov *et al.*, Phys. Rev. B **59**, 1808 (1999).
[5] N. E. Sluchanko *et al.*, Zh. Eksp. Teor. Fiz. **115**, 970 (1999) [JETP **88**, 533 (1999)].
[6] D. Mandrus *et al.*, Phys. Rev. B **49**, 16 809 (1994).
[7] O. Pena *et al.*, Solid State Commun. **40**, 539 (1981).
[8] J. C. Cooley *et al.*, Phys. Rev. B **52**, 7322 (1995).
[9] S. Nakamura *et al.*, J. Phys. Soc. Jpn. **60**, 4311 (1991).
[10] A. Kebede *et al.*, Physica B **223-224**, 256 (1996).
[11] S. Donovan, O. Klein, M. Dressel, K. Holczer, and G. Gruner, Int. J. Infrared Millim. Waves **14**, 2459 (1993).
[12] P. Wachter and G. Travaglini, J. Magn. Magn. Mater. **47-48**, 423 (1985).
[13] K. A. Kikoin and A. S. Mishchenko, J. Phys.: Condens. Matter **7**, 307 (1995).
[14] P. A. Alekseev *et al.*, J. Phys.: Condens. Matter **7**, 289 (1995).
[15] *Electron-Hole Droplets in Semiconductors*, edited by C. D. Jeffries and L. V. Keldysh (North-Holland, Amsterdam, 1983).
[16] T. Portengen, Th. Ostreich, and L. J. Sham, Phys. Rev. B **54**, 17 452 (1996).